VOL. 14, NO. 1, JANUARY 2019 ISSN 1819-6608
ARPN Journal of Engineering and Applied Sciences

www.arpnjournals.com

INVESTIGATION OF LOCAL BUCKLING FAILURE OF SIMPLY SUPPORTED COMPOSITE STEEL-CONCRETE BEAMS

Ali Manea Enad, Abdulnasser M. Abbas and Oday Adnan Abdulrazzaq
Department of Civil Engineering, College of Engineering, University of Basrah, Iraq
E-Mail: nasser21272@gmail.com

ABSTRACT

Twelve specimens of simply supported composite steel-concrete beams were analyzed to scrutinize the failure of local buckling; these specimens were loaded by the combined effect of axial compression and negative bending. Models of a three-dimensional nonlinear finite element were simulated by using ANSYS 12.1 program to estimate the ultimate loads. To investigate the adequacy of these models, a comparison was made between the gained results with past experimental work. A suitable agreement was obtained between the outcomes, in which the extreme gap for the ultimate loads is found to be approximately 8.2%. In the meantime, local buckling failure was noticed in the compression parts of the whole proposed samples, the fail begins at the web of the steel section and then propagated to the flange. On the other hand, when the concrete slab thickness increased by 20 %, the capacity of vertical load will increase by 17.8 %, while the axial load capacity increases by 5.4 %, and if the slab thickness increased by 40 %, the vertical load capacity will be 35.5 %, and the axial load increases by 10.3%.

Keywords: local buckling, composite beams, combined loading.

1. INTRODUCTION

Composite steel-concrete structures have been used widely around the world in forms of beams, columns or slabs. They were used in both buildings and bridges due to many considerations such as economy and efficiency. This type of structures allows the entire utilization of the mechanical characteristics for both steel and concrete materials, in which the concrete slab is indeed in compression, while the steel section is undergoing to tensile forces (Oehlers and Bradford, 1995). The composite performance is carried out by using stud shear connectors; these connectors are mostly welded at the upper flange of the steel beam to withstand the longitudinal slip and also to minimize the uplift.

(Ansourian, 1981), tested six continuous steel-concrete composite beams of length equals to 9 meters. Two of these specimens had finite rotation ability and were examined under harsh sagging conditions; while the other four beams were symmetrically loaded and fail by local buckling. Beams were proposed to have ductility parameter more than 1.4, and it is possible to design them by simple plastic theory without consideration of load and span configuration. Estimation was done to the resistance of vertical shear for the concrete slab at the inner supports. It is deduced that simple plastic theory which incorporating values of the full plastic moment could be used in composite continuous members consisting of built-in steel section, suitable slab and shear connectors even at cruel cases of rotation requirement.

(Vasdravellis *et al.*, 2012), studied six full-scale composite beams subjected to the combined influence of negative bending and compression axial force. The grade of the axial load, which is applied simultaneously, was increasing from lower to the higher level. On the other hand, a finite element nonlinear sample was developed and evaluated with experimental outcomes. It is found that the proposed sample was capable to anticipate the nonlinearity response and failure styles of the tested steel-concrete beams. Moreover, the developed nonlinear model was used to carry-out a chain of parametric studies on a domain of commonly in practice used composite sections. It was remarked that, when the load applied axially on the composite member, the capacity of the negative moment for the composite beam is reduced and the local buckling of the steel beam section becomes more announced.

2. LOCAL BUCKLING

Local buckling may be defined as a form which includes plate-like distortions alone, without movement of intersection lines for the closed elements of the plate. Besides that, the length of associated buckling may be considered as the shorter amongst the three buckling modes, local, distortion and global buckling (Ádány and Sándor, 2004).

However, buckling in science is a mathematical instability leading to failure, while, in theoretical meaning, buckling may be caused by abifurcation in the solution of the static equilibrium equations. Buckling is distinguished by unexpected failure for any structural member when subjected to relatively high compressive stresses, and the point of failure is located where the compressive stresses are lower than the highest compressive stress which the material is capable to resist.

3. REPRESENTATION AND MODELING OF MATERIALS

3.1 Concrete slab

The idealization of finite element model for concrete should be qualified to represent cracking, the interaction between reinforcement and concrete, crushing, and the ability of concrete to transmit the shear by aggregate interlock after cracking. In the current study, three-dimensional brick element, SOLID65, was selected to represent the concrete. This element may be marked by eight nodes each of them having three degrees of freedom:

transmission in x, y, and z-orientations. Figure-1 shows node locations, geometry, and system coordinates related to this element (Amer *et al.*, 2012).

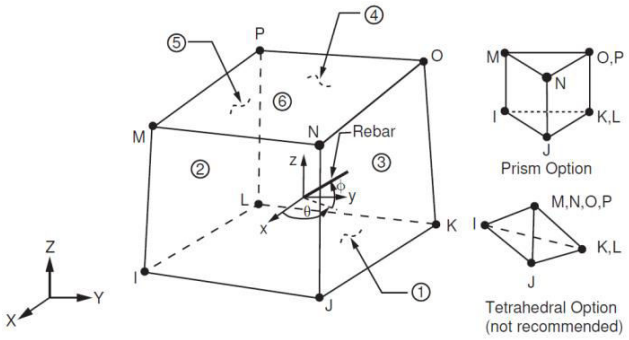

Figure-1. Geometry of SOLID65 (Amer *et al.*, 2012).

On the other hand, the modeling of concrete depends on an assumption that it is homogeneous and initially isotropic. The adopted relation of stress-strain for concrete is shown in Figure-2 (Desayi and Krishnan, 1964). While the computation of multi-linear stress-strain isotropic curve for the concrete depends on the compressive uniaxial stress-strain relationship which is obtained by using the following equations:

$f_c = \varepsilon E_c$ for $0 \leq \varepsilon \geq \varepsilon_1$ (1)

$$f_c = \frac{\varepsilon Ec}{1+(\frac{\varepsilon}{\varepsilon_0})^2} \text{for} \varepsilon_1 \leq \varepsilon \leq \varepsilon_0 \quad (2)$$

$f_c = f'_c \text{for} \varepsilon_0 \leq \varepsilon \leq \varepsilon_{cu}$ (3)

$$\varepsilon_1 = \frac{0.3\, f'c}{Ec} \text{ (Hook's Law)} \quad (4)$$

$$\varepsilon_0 = \frac{2\, f'c}{Ec} \quad (5)$$

Where:

ε_1 = strain corresponding to (0.3 f'c)
ε_0 = strain at peck point
ε_{cu} = ultimate compressive strain
Ec = Modulus of elasticity of concrete (N/ mm2)
f_c = compressive strength of concrete (MPa)
f'_c = Specified compressive strength of concrete (MPa)

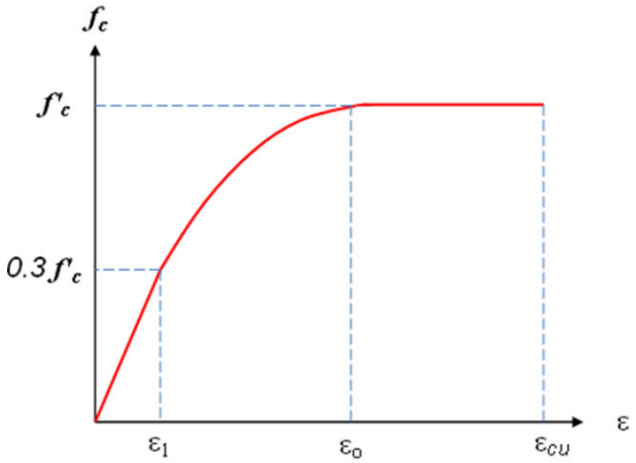

Figure-2. Simplified concrete uniaxial compressive stress-strain curve (Eurocode 3, 1993).

3.2 Steel section

The finite element simulation of the steel beam was depended on four-node, a SHELL63 element with translation in three directions x, y, and z for each node, in order to encounter the conditions of compatibility with the adjacent brick elements. The element has stress stiffening, large deflection, creep, plasticity, and considerable strain capabilities. Figure-3 shows node locations, geometry, and the system of the coordinate for SHELL63 (Amer *et al.*, 2012).

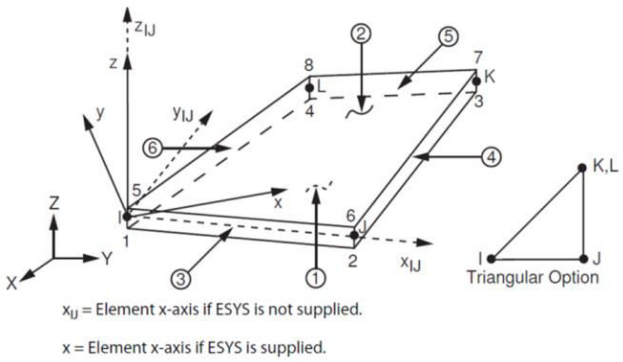

Figure-3. Geometry of SHELL63 (Amer *et al.*, 2012).

The mechanical characteristics of steel are familiar and it is much simpler in representation than the concrete. The behavior of strain-stress curve may be assumed to be congruent in both tension and compression, the relationship of bilinear stress-strain was indicated in the Figure-4 (Eurocode 3, 1993). To avert problems of convergence during iterations, the modulus of strain hardening (Et) is presupposed to be (0.03 Es), where Es is defined as the Modulus of elasticity for the steel.

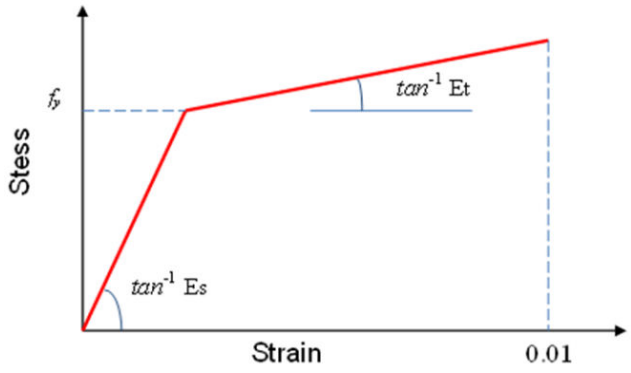

Figure-4. Stress-strain bilinear relationship for steel (Kemp *et al.*, 1995).

3.3 Steel rebar

In this study, a discrete simulation of element LINK8 was used to represent the steel rebar in the finite element model. A spar element LINK8 may be used to simulate sagging cables, links, trusses, springs, etc. This element is a tension-compression uniaxial, while each node has a freedom translation in three directions x, y, and z, and there is no bending considered for this element. Figure-5 shows node locations, geometry, and the system coordinates for the element (Amer *et al.*, 2012).

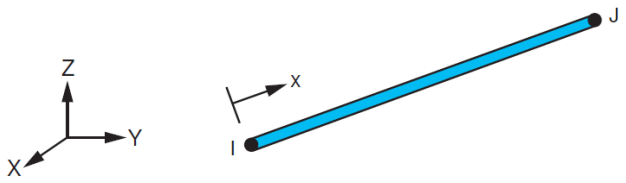

Figure-5. Geometry of LINK8 (Amer *et al.*, 2012).

Because the ordinary steel bars are considered as a slender they may be presupposing to transfer axial force only. The steel rebar modeling in the finite element is very simple; however, the stress-strain curve for steel rebar can be simulated in Figure-4.

3.4 Shear connectors

The nonlinear behavior of shear connectors is simulated by using spring COMBIN39 and LINK8 elements. The element COMBIN39 is used to work against normal forces between steel section and concrete while element LINK8used as stirrups to resist perpendicular shear at the concrete layer. The element COMBIN39 is unidirectional with the generalized nonlinear force-deflection ability that could work in any analysis. This element has torsional or longitudinal capability for application of one, two, and three-dimensions. The element node locations, geometry, and system of coordinates are shown in Figure-6 (Amer *et al.*, 2012).

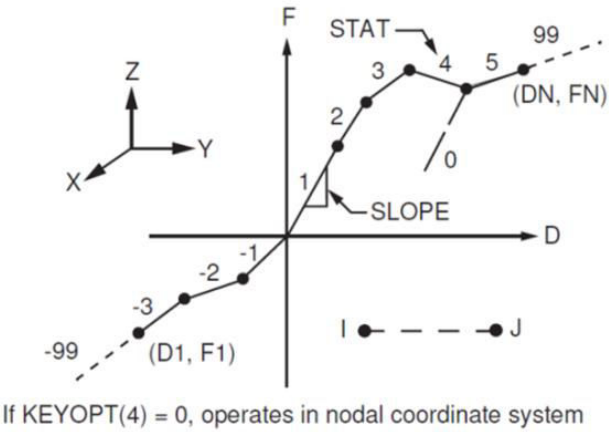

Figure-6. Geometry of COMBINE39 (Amer *et al.*, 2012).

The major assignment of the connectors is to transfer the shear force between concrete slab and steel section; this force may be computed depending on the following equation (Kemp *et al.*, 1995):

$$F_d = a(1-e^{-bu_c}) \quad (6)$$

where:

F_d = stud connector shear force,
u_c = slip,
b = constant,
a = ultimate shear resistance of stud shear connector.

3.5 Steel plates

To prevent stress concentration it is preferable to use steel plates at the loading and support positions. These plates guarantee the distribution of stresses over the loading area. Element SOLID45 is used to simulate the steel plates, this element could be used in the modeling of three dimensional structures. It is defined by eight nodes, each one of them having translation in the three directions x, y, and z, as shown in figure (7) (Amer *et al.*, 2012).

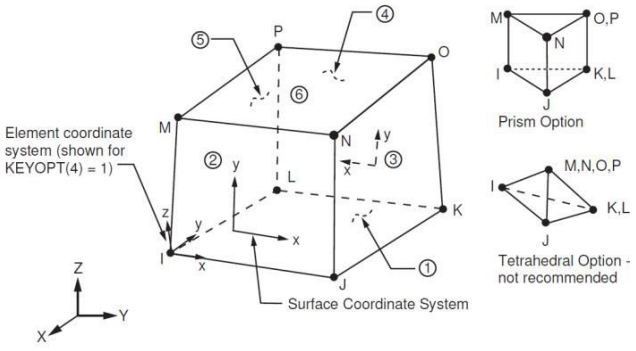

Figure-7. Geometry of SOLID45 (Amer *et al.*, 2012).

3.6 Interface element

The space between concrete and steel section is represented by CONTAC52 element with two surfaces that may preserve or break the physical contact and could

slide relatively over each other. Moreover, each node of this element has free to translate in x, y and z directions.

4. GENERAL NONLINEAR SOLUTION

When static problems are solved by finite element method, a series of linear simultaneous equations are gained in the form of (Amer *et al.*, 2012):

$$[K].\{a\}=\{f\} \quad (7)$$

These equations may be directly obtained for problems of the simple elastic solution, however, the solution becomes difficult to achieve if the nonlinearity is submitted for the stiffness matrix [K]. This matrix is mainly depends on displacement {f} = [K] {a}, and therefore cannot be calculated exactly before founding the nodal displacement unknowns {a}. In the present study, the nonlinear solution for the problems is attained by using the technique of incremental-iteration; this technique is used widely in the analysis, especially for the concrete nonlinear problems.

5. CONVERGENCE CRITERIA

If the strategy of any solution that depends on the iterative methods is efficient, then, the terminus of the iteration should be based on factual criteria. The solution obtained by the end of any iteration must be checked to observe the convergence. When the convergence allowance is too loose, incorrect outcomes are gained, while, when the tolerance is too strict, many computational operations effort is done to gain the required accuracy.ANSYS program allows many choices for convergence criterion which may be based on forces, displacements or rotations, moments, or any combination of them. Moreover, each of these items can govern by various values of convergence tolerance. In this study, the force criterion was used to govern the analysis.

6. COMPARISON STUDY

To demonstrate the efficiency of the proposed finite element models, a compression is done between the gained outcomes form the numerical analysis with previous experimental work (Jianguo and Yan, 2004) for ultimate loads. The major parameters of the experimental work were shear span length, width, and thickness of the concrete slab. Shear span ratio may be defined as the length of span over the entire composite beam height, this ratio changed from 1.0 to 4.0. The major details of the beams are shown in Table-1.

Table-1. Details of composite beams used in the experimental work (Jianguo and Yan, 2004).

Beam no.	λ	h_f (mm)	b_f (mm)	a (mm)	Span length (mm)	Transverse steel	Stud height (mm)	f'_c (Mpa)	f_y (Mpa)
CBS-1	1	100	680	300	2800	Φ8-90*	85	32.85	273
CBS-2	2			600				30.06	
CBS-3	3			900		Φ8-55		32.64	
CBS-4	4			1200		Φ8-60	105	36.98	
CBS-5	1	120		320		Φ8-100		29.73	
CBS-6	2			640				35.85	
CBS-7	3			960		Φ8-60		31.16	
CBS-8	4			1280		Φ8-65		35.98	
CBS-9	1		480	320	2000	Φ6-60		31.60	
CBS-10	2			640				36.65	
CBS-11	3			960	3000	Φ8-55		35.91	
CBS-12	4			1280		Φ8-65		38.54	
CBS-13	1	140		340		Φ6-60	125	38.13	
CBS-14	2			680				36.14	
CBS-15	3			1020		Φ8-65		33.30	
CBS-16	4			1360		Φ8-70		30.66	

*1. Φ8 at 90mm $^c/_c$.
2. λ=shear span ratio, λ=*a*/*h*, *a* and *h*=shear span and height of the composite beam.

7. PARAMETRIC STUDY

A group of steel-concrete beams consist of twelve specimens was selected to investigate the failure of local buckling. A combination of axial compression force and positive bending were applied to these specimens. Each one of these composite beams constitutes of concrete slab and universal steel section, UB203x133x30, connected together by stud shear connectors. The major considerable

parameters used in this study were, concrete slab width and thickness, and transverse reinforcement quantity.

In order to avoid stress concentration and to prevent the buckling of web, steel plates of 15 mm thick were modeled as stiffeners at supports and load application points to reduce stress concentration, see Figure-8.

The study considered four groups of composite beams, group1 to group 4, these groups having effective length of 3 m, 2.8 m, 2.6 m, and 2.4 m, respectively. Beams details are shown in Table-2.

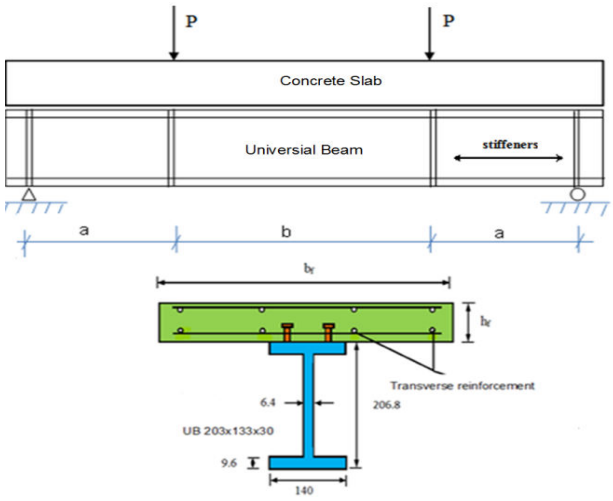

Figure-8. Details of composite beam and loading conditions.

Table-2. Details beams used in the current study.

Beam no.	h_f (mm)	b_f (mm)	Span length (mm)	Transverse steel	Stud height (mm)	f'_c (Mpa)	f_y (Mpa)
CB-1	100	680	3000	Φ6-100	85	25	410
CB-2	120				105		
CB-3	140				125		
CB-4	100	600	2800	Φ6-90	85		
CB-5	120				105		
CB-6	140				125		
CB-7	100	540	2600	Φ6-80	85		
CB-8	120				105		
CB-9	140				125		
CB-10	100	480	2400	Φ6-70	85		
CB-11	120				105		
CB-12	140				125		

8. CONSTRUCTED MESH

In the current investigation, rectangular or square elements were used in order to gain relatively accurate outcomes. However, meshing was not needed for steel rebar because it is considered as a single element that constructed over the nodes through the volume mesh of the concrete. Figures (9) and (10) illustrate the rebar structure and meshing for the steel-concrete beam.

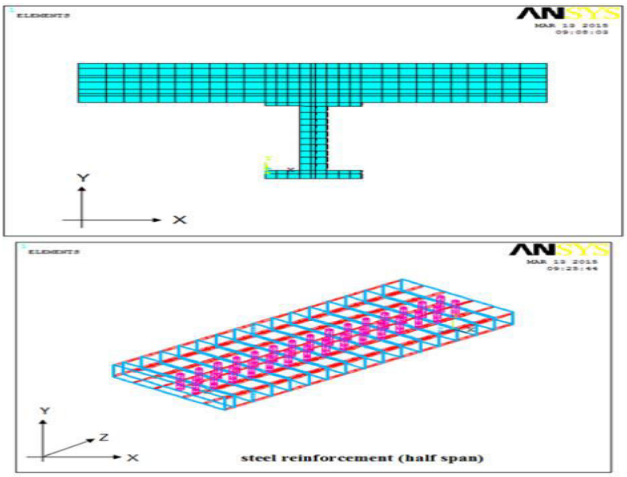

Figure-9. Representation of composite beam in x-y plane and steel reinforcement.

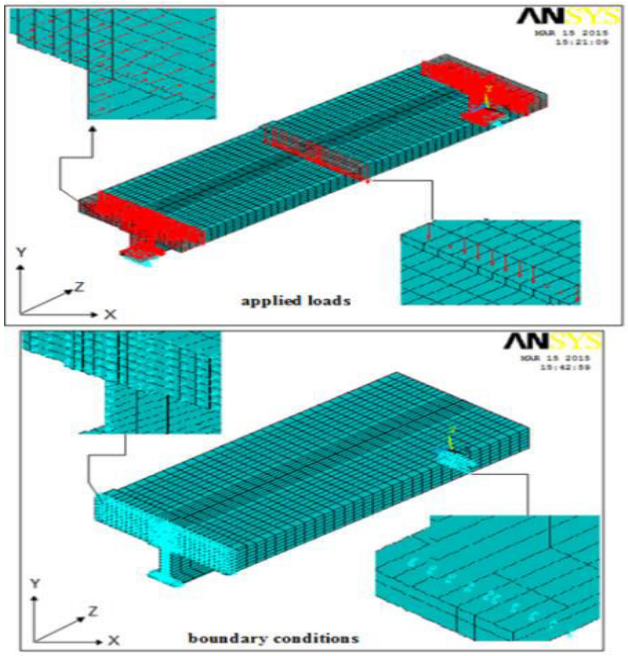

Figure-10. Representation of applied loads and boundary conditions (half span).

The influence of element type and mesh density on the outcomes was performed. To obtain sufficient convergence for the results, the number of elements that used in a structure increased until reaching to a certain number in which the increase of these elements shows the negligible effect on the gained outcomes.

Due to the symmetry in geometry and loading, only a half-span for each specimen was considered. This action will simplify the analysis and reduce the calculations. For each sample, thirty elements were taken in the z-direction for both slab and beam, while taken number of elements in x and y-directions were stated in Table-3.

Table-3. Number of used elements in x and y-direction for all specimens.

Beam no.	x- direction		y-direction	
	CS[1]	UB[2]	CS	UB
CB-1	29	9	6	12
CB-2			7	
CB-3			8	
CB-4	27		6	
CB-5			7	
CB-6			8	
CB-7	25		6	
CB-8			7	
CB-9			8	
CB-10	23		6	
CB-11			7	
CB-12			8	

[1]Concrete Slab, [2]Universal Beam

9. DISCUSSION OF OUTCOMES

9.1 Ultimate load

In the finite element problems, the computation of ultimate load depends utterly on the final step of loading, moreover, the solution becomes diverges due to initiating of cracks and considerable deformations. In the current work, comparisons were done between ultimate loads gained from the proposed solution P_{Num} with the values that obtained from the past experimental work P_{Exp} (Jianguo and Yan, 2004), see Table-4. From these data, it can be seen that the values of experimental to numerical ratios are changed from 0.934 to 1.089 with an average of 1.007, and the upper gap between the experimental to the finite element ultimate loads is 8.2%.

On the other hand, when the concrete slab thickness raised by 20%, the capacity of vertical load will increases by 17.78% and the capacity of axial load also increased by 5.43%, in the same manner, if the slab thickness increases by 40%, the vertical load raises by 35.53% and while the axial load raised by 10.26%.

Table-4. Values of the ultimate loads for numerical and experimental studies.

Beams	Ultimate load (kN)		$P_{exp.}/P_{num.}$	$(\frac{Pexp.-Pnum.}{Pexp.})\%$
	$P_{exp.}$	$P_{num.}$		
CBS-1	453	439	1.033	3.1
CBS-2	355	351	1.011	1.1
CBS-3	275	281	0.979	2.1
CBS-4	211	200	1.055	5.2
CBS-5	483	473	1.021	2.1
CBS-6	367	378	0.971	2.9
CBS-7	291	303	0.960	4.0
CBS-8	235	237	0.992	1.0
CBS-9	497	482	1.031	3.0
CBS-10	399	396	1.008	1.0
CBS-11	266	261	1.019	2.0
CBS-12	207	190	1.089	8.2
CBS-13	537	563	0.954	4.6
CBS-14	422	405	1.042	4.0
CBS-15	271	290	0.934	6.6
CBS-16	205	203	1.010	1.0

Table-5 shows the ultimate loads gained from the finite element analysis for composite steel-concrete beams loaded by combined positive bending and axial force. Form this table; it is found that, the common mode of failure for all studied specimens was the local buckling. First of all, the failure starts from the steel section especially in the web and then it is extended to the flange, in the meantime, significant cracking was observed in the concrete slab at the same zone.

Table-5. Numerical values of ultimate loads and failure mode.

Beams	Ultimate load (kN)		Type of failure
	Vertical	Axial	
CB-1	191	1488	Local Buckling
CB-2	224	1567	
CB-3	261	1625	
CB-4	184	1350	
CB-5	218	1431	
CB-6	249	1483	
CB-7	173	1178	
CB-8	200	1233	
CB-9	230	1296	
CB-10	152	1007	
CB-11	182	1064	
CB-12	208	1128	

9.2 Stresses and strains distribution

Stains are increased gradually when the applied load increases due to stresses redistribution on the cracked elements.

Stresses distribution contours at ultimate load stage along some of the studied specimens are shown in Figure-11; stresses were changed from 644.176 N/mm^2 to 807.410 N/mm^2 with 746.363 N/mm^2 as an average value.

On the other hand, Figure-12 illustrates strains distribution contours for some tested beams at ultimate load, in which the strain maximum values were varied from 0.003464 to 0.004544 with 0.003823 as an average.

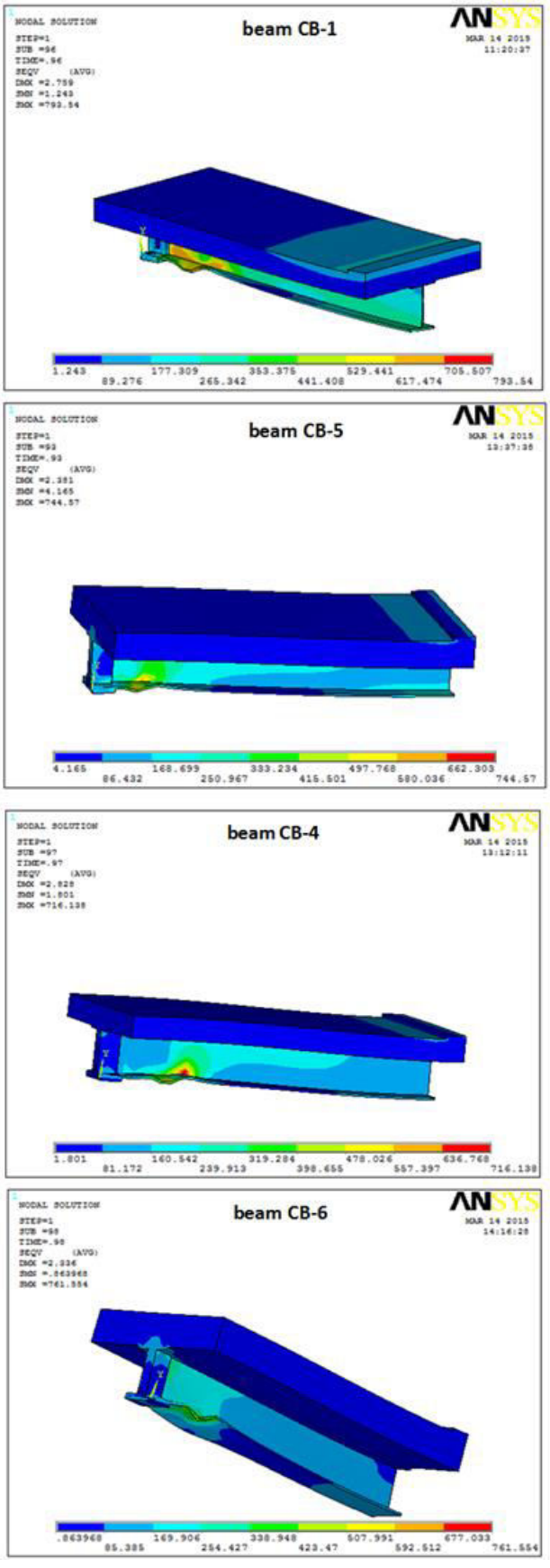

Figure-11. Stress distribution in Z-direction along half span at ultimate load.

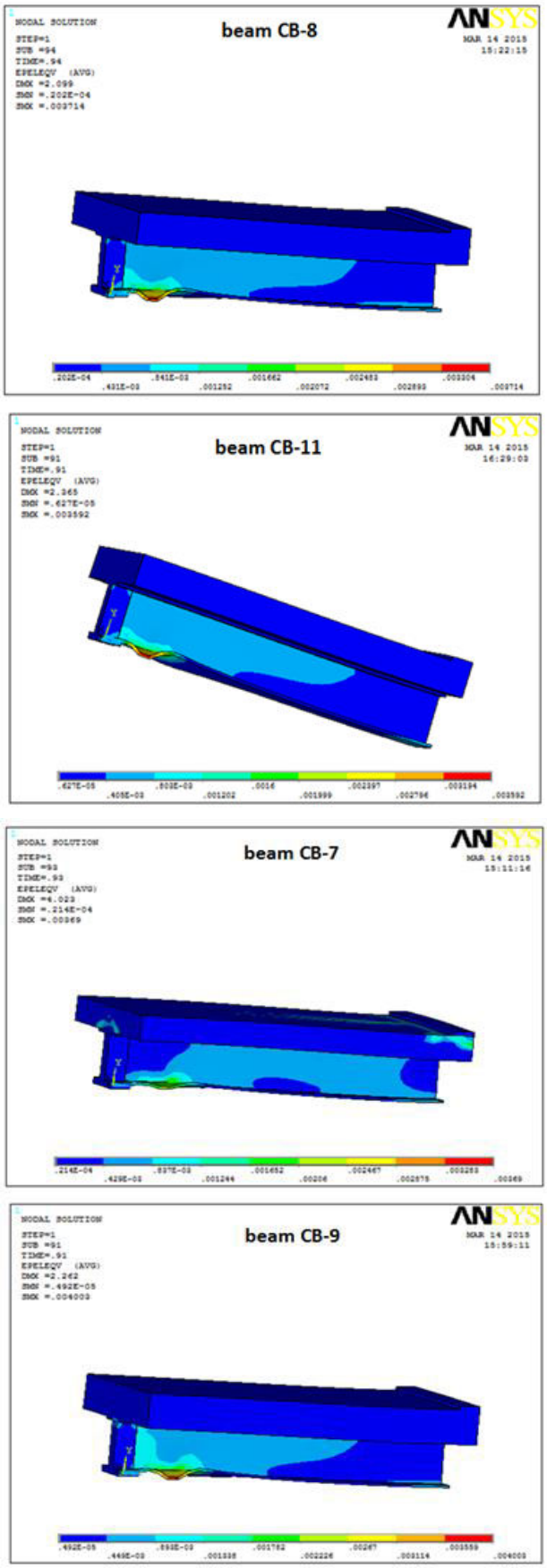

Figure-12. Strain distribution in Z-direction along half span at ultimate load.

10. CONCLUSIONS

a) The presence of axial compression force accelerates the local buckling failure.
b) In order to minimize local buckling, stiffener plates were provided for flanges and webs of the steel section at loading and support parts.
c) By using the finite element technique, a nonlinear problem of three-dimensional model can be developed effectively to examine the structural behavior and modes of failure for composite steel concrete beams subjected to combined bending and axial force.
d) A maximum gap of approximately 8.2% is found between the past experimental outcomes with the present numerical ultimate loads.
e) As the stiffness of the composite beam enhanced, the capacity of holding loads will consequently improve, therefore, the increasing o-f concrete slab thickness by 20% leads to increasing of vertical load capacity by 17.8% and the axial load will also increase by 5.4%, while, it is increased by 40%, the vertical load and the axial load raised by 35.5% and 10.3%, respectively.

REFERENCES

Oehlers D. J., and Bradford M. A. 1995. Composite steel and concrete structural members: Fundamental behaviour. Pergamon, Tarrytown, N.Y., USA.

Ansourian P. 1981. Experiments on continuous composite beams. Research Report No. R384, University of Sydney, March.

Vasdravellis G., Uy B., Tan E.L. and Kirkland B. 2012. Behaviour and design of composite beams subjected to negative bending and compression. University of Western Sydney, Sydney, Australia.

Ádány and Sándor. 2004. Buckling Mode Classification of Members with open Thin-walled Cross Sections by using the finite strip method. Johns Hopkins University.

Amer M. Ibrahim, Saad k. Mohaisen, and Qusay W. Ahmed. 2012. Finite element modeling of composite steel-concrete beams with external prestressing. International Journal of Civil and Structural Engineering. 3(1).

Desayi P. and Krishnan S. 1964. Equation for the stress-strain curve of concrete. Journal of the American concrete institute. 61: 345- 350.

1993. European Committee for Standardization (CEB), Eurocode 3, Design of steel structures, Part 1.1: General rules and rules for buildings, DD ENV, 1-1, EC3.

Kemp A.R., Dekker N.W. and Trinchero P. 1995. Differences in Inelastic Properties of Steel and Composite Beams. Journal of Constructional Steel Research. (34): 187-206.

Jianguo Nie and Yan Xiao. 2004. Experimental Studies on Shear Strength of Steel-Concrete Composite Beams. Journal of Structural Engineering, August.